Vertex Effect in Strain-Softening Concrete at Rotating Principal Axes

Ferhun C. Caner[1]; Zdeněk P. Bažant, F.ASCE[2]; and Jan Červenka[3]

Abstract: The inelastic behavior of concrete for highly nonproportional loading paths with rotating principal stress axes is studied. Test cylinders are first loaded in compression under uniaxial stress and then torsion is applied at constant axial displacement. Proportional compressive-torsional loading tests are also carried out for comparison. The tests demonstrate that the response of concrete for load increments parallel in the stress space to the current yield surface is highly inelastic (i.e., much softer than elastic) in the peak load range and especially in the postpeak range. The classical tensorial models of plasticity type incorrectly predict for such load increments the elastic stiffness. The experiments are simulated by three-dimensional finite element analysis using the microplane model M4, in which the stress-strain relations are characterized not by tensors but by vectors of stress and strain on planes of various orientations in the material. It is shown that the observed vertex effect is correctly predicted by this model, with no adjustment of its material parameters previously calibrated by other test results. The experiments are also simulated by a state-of-the-art fracture-plastic model of tensorial type and it is found that the vertex effect cannot be reproduced at all, although an adjustment of one material parameter suffices to obtain a realistic postpeak slope and achieve a realistic overall response. What makes the microplane model capable of capturing the vertex effect is the existence of more than 60 simultaneous yield surfaces. Capturing the vertex effect is important for highly nonproportional loading with rotating principal stress axes, which is typical of impact and penetration of missiles, shock, blasts, and earthquake.

DOI: 10.1061/(ASCE)0733-9399(2002)128:1(24)

CE Database keywords: Inelastic action; Concrete; Nonproportional loads; Rotation.

Introduction

As a convenient way of avoiding material instability, the incremental theory of plasticity is based on Drucker's (1950) postulate. This postulate requires the inelastic strain increment vector to be normal to the yield surface in the superposed nine-dimensional spaces of stress and strain components. Adherence to the normality rule (expounded, e.g., in Bažant and Cedolin 1991, Chapter 10) is the basic feature of all the practical constitutive relations for plasticity of metals. The normality rule is also adopted for the fracturing (Dougill 1976) and plastic-fracturing constitutive models for concrete with loading surfaces in the strain space (Bažant and Kim 1979; Lin et al. 1987; Červenka et al. 1998).

The normality rule implies that, for load increments that are parallel to the current yield surface (or loading potential surface), called the ''loading to the side,'' the response is purely elastic. Such behavior was rendered doubtful by Bleich's (1952) tests of plastic buckling of plates and was shown patently untrue by Gerard and Becker (1951, 1957), who tested axially compressed thin-walled cruciform steel columns that buckle in the plastic range by torsion. The critical load of such columns is proportional to the tangential inelastic stiffness for loading to the side, and it was found that it can be much smaller than the critical load for the elastic stiffness—even less than one half of the elastic critical load (Bažant and Cedolin 1991, Sec. 8.1; in detail Brocca and Bažant 2000a,b). This means that the response for loading to the side is inelastic.

The existence of inelastic strain increments for loading to the side implies that there must be a corner, or vertex, on the yield surface (or loading potential surface) at the current state point, traveling during loading with the state point as the material hardens or softens. Therefore, the phenomenon is called the ''vertex effect'' (Jirásek and Bažant 2002). The vertex effect is the strongest for abrupt changes of loading direction in the stress space or strain space, but arises for all loading paths (even smooth paths) significantly deviating from proportional loading (radial loading in the stress or strain space).

The vertex effect is particularly marked when the principal strain or stress axes rotate against the material (Bažant 1983). This happens when the strain (or stress) increment has shear components with regards to the principal axes of the current strain or stress tensor. For nonproportional loading paths without rotation of the principal axes, which are the only nonproportional paths observable in the so-called ''true'' (cubical) triaxial tests, the vertex effect appears to be either weak or nonexistent.

The purposes of this paper are to (1) present new experimental results that clearly document the existence of the vertex effect in concrete for paths with rotation principal axes, (2) show that the vertex effect is correctly predicted by the microplane model (par-

[1]Assistant Professor, Mustafa Kemal Univ., Muhendislik ve Mimarlik Fakultesi, 31230 Iskenderun, Turkey; formerly, Graduate Research Assistant, Northwestern University, Evanston, IL 60208.

[2]Walter P. Murphy Professor of Civil Engineering and Materials Science, Northwestern University, Evanston, IL 60208. Email: z-bazant@northwestern.edu

[3]Červenka Consulting Co., Prague, Czech Republic; formerly Visiting Scholar, Northwestern Univ., Evanston, IL 60208.

Note. Associate Editor: A. Rajah Anandarajah. Discussion open until June 1, 2002. Separate discussions must be submitted for individual papers. To extend the closing date by one month, a written request must be filed with the ASCE Managing Editor. The manuscript for this paper was submitted for review and possible publication on July 18,2000; approved on February 21, 2001. This paper is part of the ***Journal of Engineering Mechanics***, Vol. 128, No. 1, January 1, 2002. ©ASCE, ISSN 0733-9399/2002/1-24–33/$8.00+$.50 per page.

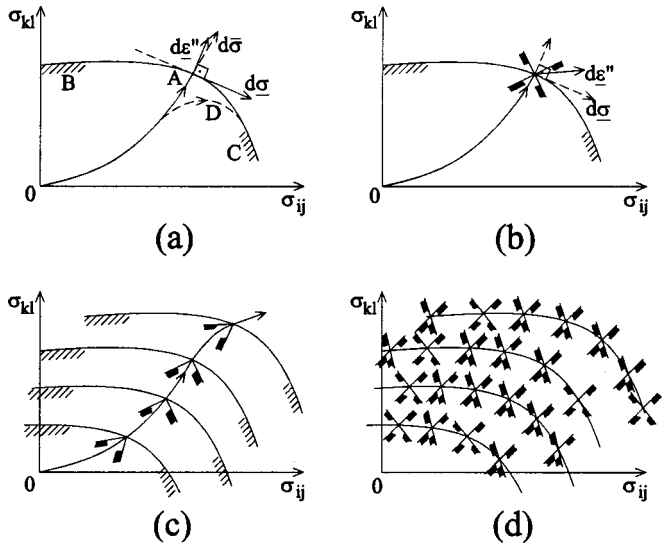

Fig. 1. Vertex effect and associated difficulties: (a) Yield surface for classical plasticity with normality; (b) multiple yield surfaces at the state point and loading to the side; (c) concept of traveling vertex; and (d) multiple yield surfaces at every state point, required for capturing the vertex effect in the context of classical plasticity

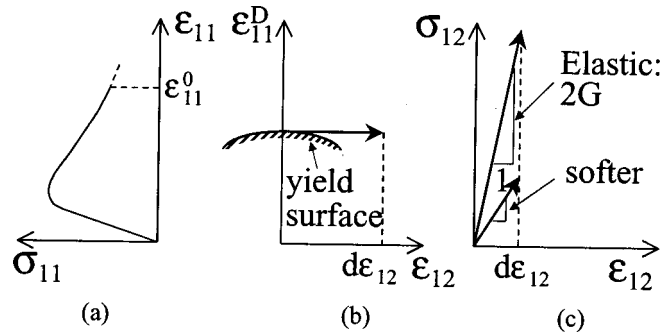

Fig. 2. Typical representation of vertex effect in concrete: (a) deviatoric loading with no shear strains; (b) subsequent pure shear loading which is tangent to the yield surface in the space of deviatoric strains; and (c) response to the pure shear loading predicted by plasticity-based models, which is elastic (with slope $2G$) and much stiffer than observed

ticularly its latest version; Bažant et al. 2000; Caner and Bažant 2000), and (3) make a comparison with one advanced concrete model of plastic tensorial type (Červenka et al. 1998).

Vertex Effect and Associated Difficulties

To explain the vertex effect, consider point *A* of the loading path *OA* lying on the current yield surface *BAC* (or loading potential surface) in stress space (Fig. 1) or strain space. When the loading continues smoothly with stress increment vector $d\bar{\boldsymbol{\sigma}}$, there is finite inelastic strain increment $d\bar{\boldsymbol{\epsilon}}''$. According to the normality rule, ensuing from Drucker's postulate (e.g., Bažant and Cedolin 1991, Chap. 10), the nine-dimensional vector $d\bar{\boldsymbol{\epsilon}}''$ is normal to the yield surface, which must be considered as a surface in the nine-dimensional space of stress or strain components (marked as σ_{ij} or σ_{kl}). But this means that when the stress increment $d\boldsymbol{\sigma}$ is tangential to the yield surface (loading to the side, Fig. 1), there is no inelastic strain and thus the response is purely elastic.

This incorrect property, proven wrong for metals by the aforementioned famous experiments of Gerard and Becker (1951; 1957), can be avoided, in the context of plasticity-type theories, by assuming that there exists a sharp corner (or vertex) at the current yield surface at any current state point *A* [Fig. 1(b)]. This means that there must exist further intersecting yield surfaces at point *A*, which cause that the inelastic strain increment $d\bar{\boldsymbol{\epsilon}}''$ normal to this surface has a nonzero component in the direction of loading to the side (Fig. 1) and the response is then softer than elastic.

In general, the vertex effect develops for any significant deviations from proportional loading, for example the smooth path *ODC* shown in Fig. 1. The vertex effect creates enormous difficulties with the classical tensorial models of plasticity (Jirásek and Bažant 2002). It has been intensely debated in the literature up to the mid-1980s, but then the interest waned, apparently out of frustration. No tensorial models exhibiting the vertex effect are available for large-scale finite element analysis in which, for metals, von Mises J_2 plasticity still dominates.

One way to cope with the vertex effect has been to assume a so-called "traveling vertex," i.e., a vertex on the current yield surface that travels with the current state point along the loading path [Fig. 1(c)]. Such vertex enhancements of classical plasticity have been formulated for characterizing the first infinitesimal deviation from the proportional loading path and were used to study the bifurcation instabilities at the onset of localization of yielding into shear bands (Rice 1975, 1976; Rudnicki and Rice 1975; Christoffersen and Hutchinson 1979; Hughes and Shakib 1986). These approaches, however, are not effective for predicting what happens afterwards, after large deviations from the previous loading direction in the stress or strain space take place.

Hencky's deformation theory of plasticity was found to predict an approximately correct vertex behavior for initial infinitesimal deviations from a proportional loading path with rotation of principal axes [e.g., it gives approximately correct predictions for the tests of Gerard and Becker (1951, 1957); see Budianski (1959)]. But since this theory represents a path-independent model, it cannot be used for highly nonproportional loading path. The endochronic theory, which represents an incrementally nonlinear modification of plasticity, does provide vertex behavior for arbitrary nonproportional paths (Bažant 1978), but has no physical basis and turned out to be less powerful than the microplane model.

A nonassociated flow rule cannot be used to simulate the vertex effect. It does yield inelastic response for loading to the side, but only to one side. To illustrate it, consider the state point $\epsilon_{11}^D > 0$, $\epsilon_{12} = 0$ in Fig. 2(b). To obtain an inelastic response for moving from this point to the right (i.e., in the positive ϵ_{12} direction), the slope of the loading surface that controls the flow rule would have to be at that point negative, but then the response for moving from that point to the left would be predicted as elastic. Besides, the nonassociativeness is a feature used typically for the volumetric-deviatoric interactions, while the vertex effect occurs not only, and not mainly, in the volumetric-deviatoric cross sections of the stress space, but also, and mainly, in the deviatoric stress space alone.

The physical source of the vertex effect has been clarified by various sophisticated models for polycrystalline metals, especially the slip theory of plasticity of Batdorf and Budiansky (1949) and further refinements of Taylor's (1938) model (Budiansky et al. 1951; Naghdi et al. 1958; Ivey 1961; Phillips and Gray 1961;

Bertsch and Findley 1962); for a detailed review see Brocca and Bažant (2000a,b). The vertex effect is caused by the development of multiple yield (or loading potential) surfaces. Many surfaces are active simultaneously (Fig. 1) (Phillips 1972, 1986). After a sudden change of the loading path direction in the stress or strain space with rotation of the principal axes (i.e., when the incremental strain has nonzero shear components with regard to the current principal axes), some yield surfaces suddenly go into unloading and deactivate while others suddenly become active. Whereas the vertex effect plays no role for proportional loading and is insignificant or nonexistent for nonproportional loading with fixed principal stress axes (as in ''true,'' or cubical, triaxial tests), it is very important for highly nonproportional loading with rotating principal stress axes. Such a loading typically arises in dynamics, for example in problems of impact or penetration of missiles, shock, and blast effects on hardened structures, and earthquake effects on buildings or bridges.

Formulations of multisurface plasticity within the context of the classical tensorial models with invariants are available (Koiter 1953) but difficult to implement and identify from test data, particularly when there are more than just two or three separately evolving loading surfaces. No plasticity type models with many loading surfaces (Fig. 1) exist. For soils, there exist models involving two yield surfaces (one for the deviatoric space and one for the coupling with mean stress), but for capturing the vertex effect, two yield surfaces are insufficient by far (the number of yield surfaces implied by the microplane model M4 is about 60, which is what seems necessary for capturing the vertex effect in general).

Multisurface models become conceptually simple with the general approach proposed for metal plasticity by Taylor (1938), and later adapted to frictional plastic-fracturing behavior of concrete with softening damage under the name microplane model (Bažant 1983). What achieves simplicity is that the stress-strain relations are formulated in terms of vectors rather than tensors. The vectorial form makes it easier to reflect physical phenomena such as friction and cracking. Exploration of this approach to the vertex effect in concrete is the subject of this paper.

Tests of Vertex Effect in Concrete and Response at Rotating Principal Axes

To examine the vertex effect in concrete at rotating principal axes, one may use as a typical example the loading path illustrated in Fig. 2. A uniaxial compressive strain is initially applied [Fig. 2(a)], which represents proportional loading. No shear strains develop during this loading. The state of loading on the yield surface for macroscopic plasticity is as shown in Fig. 2(b). A sudden imposition of incremental shear strain, shown in the figure, represents ''loading to the side'' and causes the principal stress direction to rotate. The response to such loading is depicted in Fig. 2(c). The existing tensorial plasticity models in terms of stress and strain invariants inevitably follow the curve whose initial slope is in the figure shown as $2G$, while the real material response is much softer, as shown in the figure.

The experiments are designed for cylindrical specimens so that they can be tested in an axial-torsional testing machine. The load path is prescribed in the space of axial displacement versus rotation, and the response in the postpeak regime is of interest. The loading path includes a sharp corner. A rounded corner can be avoided thanks to the availability of a-state-of-the-art testing machine.

Cylindrical specimens of concrete with diameter $D=4$ in. (101.6 mm) and height $H=8$ in. (203.2 mm) are used. These dimensions correspond roughly to the representative volume of the material (the smallest volume in which it can be treated as a continuum). The experiment is delicate. It requires a very responsive closed-loop digital feedback testing machine capable of applying both axial displacements and rotations, and the displacements need to be measured on a specimen that is *softening*. Furthermore, the gauge range must be estimated so that the accruing damage would stay within that range. To minimize end effects, the gauges must be attached to the specimen. Since carrying out the experimental program takes several weeks, and all the specimens must be cast from the same batch of concrete, the ages of specimens differ. The relative age differences, which is what counts, are therefore minimized by allowing a long enough curing period.

The specimens are made of normal strength concrete obtained by mixing 339.5 kg of Type-I Cement, 949.7 kg of pea size coarse aggregate with a maximum aggregate size of 9.5 mm, 887.2 kg of sand No. 2, and 201.8 kg of water per cubic meter. The larger size aggregates consist of dolomite, granite, and basalt, with trace amounts of schist. The specimens cast are cured in a fog room for 5 months before testing. The purpose of such a long curing period is to minimize the differences between the specimens tested at the beginning and the end of the three-week testing program. According to model B3 (Bažant and Baweja 2000), the difference in strength due to aging should be only about 2.5%, but it would be about 18% if the three-week testing program started at concrete age 1 month.

If a sudden switch from uniaxial compressive loading to torsional loading is made at prepeak stress less than about 40% of the compressive peak stress, the response is elastic and path independent. Even at higher prepeak stresses, the response is nearly path independent. Therefore the vertex effect is tested only in the peak and postpeak regions.

To test the vertex effect in the peak region, the specimen is compressed under uniaxial stress (at zero rotation) to strain $\epsilon = 0.2\%$ (which is the axial strain at maximum uniaxial stress $\sigma = f_c'$ for a typical concrete). This is followed by concentric rotation at constant axial strain $\epsilon = 0.2\%$ until the peak torque is reached. Of main interest is the case when the switch to torsion is made in the *postpeak* regime. The concrete specimen is compressed axially at zero rotation to the strain 0.45%, which is followed by concentric rotation until the peak torque is reached while keeping the axial strain constant.

For comparison, proportional (radial) loading paths, in which the rotation is increased simultaneously and in proportion to the axial displacement until the specimen fails, are also used. The ratio of displacement to rotation in these tests is kept as $u/\phi = 100$ mm/rad.

The load paths used in all the tests are graphically shown in Fig. 3. The reason for choosing load paths with prescribed displacement rather than loads is obvious; under load control, the postpeak regime of concrete response is unstable (e.g., Bažant and Cedolin 1991) and could not be accessed. A path in which the specimen would first be subjected to rotation at constant axial displacement and then to axial displacement at constant rotation is not used because rotations large enough to cause damage in the absence of axial compression would also lead to fracture.

The ratio of axial strain to torsional rotation is determined so that the radial path and the path with a corner would intersect at a point of high damage but before the specimen fails. Slightly higher or slightly lower ratios would not satisfy this objective. Based on preliminary tests, the optimal axial compression and

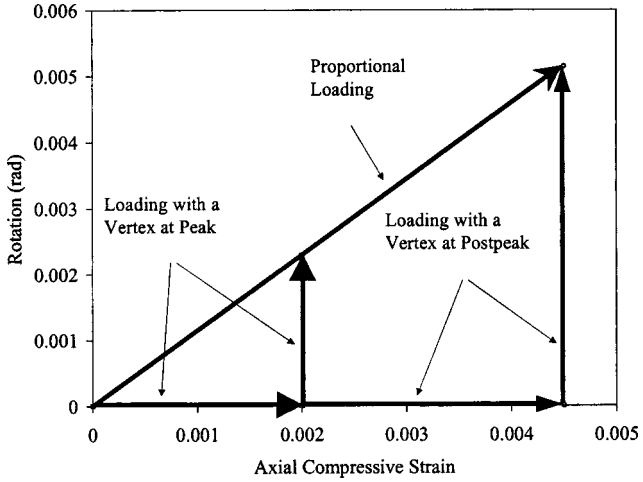

Fig. 3. Load paths prescribed in the experiments

rotation rates are fixed as 3.33×10^{-4} mm/s and 3.33×10^{-6} rad/s, respectively.

The specimen is embedded into steel platens at the top and bottom ends to a depth of 12.7 mm. The concrete is glued to the platens by a high-modulus epoxy (SIKADUR 32 HI-MOD). This means that the ends of the specimen are confined and so the failure processes take place not at the ends but within the gauge region. The glue is strong enough to transfer the torque into the specimen. The specimens are glued to the platens in situ, i.e., while the platens are already attached to the testing machine. This guarantees the initial state to be free of bending moments and end rotations about horizontal axes. If the platens were glued before installation in the machine, they would hardly be perfectly aligned and bending moments would be introduced at the specimen ends. The top platen is bolted to the load cell.

Because of deformation of the glue and the lateral restraint of concrete by the platens, as well as the complex nonlinear behavior of concrete near the platens, the stroke (the relative axial displacement of the platens) cannot be used as a measure of the axial deformation of displacement of the specimen. Therefore, the specimen is externally instrumented to obtain the axial displacements and rotations in the central portion of the specimen, far enough from the end restraints. To this end, two linear variable differential transformers (LVDTs) for axial loading and two LVDTs for rotational loading are used as shown in Fig. 4. These LVDTs are mounted on the two steel rings attached directly to the specimen at the top and bottom of the gauge volume, each by four screws. The LVDTs used for measuring the axial displacements over a gauge length of $L=114.3$ mm had the range of ±2.54 mm. The rotational LVDT have the range ±0.508 mm, and the distance between the rotational LVDTs is 95.25 mm. The difference in the readings of the two axial LVDTs can reveal possible bending of the specimen. Since the experiments are performed by prescribing the average value of the two axial LVDT readings, any specimen with significant bending moments gets crushed by the test machine because in that case the average of the two axial LVDTs cannot be kept constant while torsional rotation is applied.

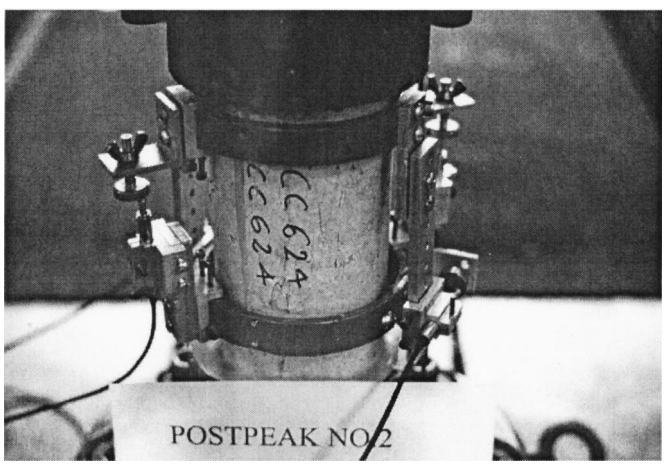

Fig. 4. Experimental setup for axial-rotational loading (the relative axial displacements and rotations of top and bottom rings are measured using two sets of LVDTs)

Table 1. Basic Results from Experiments

Loading	Specimen number	E (GPa)	f_c' (MPa)	$K_{\text{rotational}}$ (kN m/rad)	$T_{\max}$ (kN m)
Proportional	1	37.370	⋯	1449	1.295
	2	36.922	⋯	1422	1.191
	3	37.499	⋯	1419	1.015
	4	36.400	⋯	1444	1.268
Vertex at $\sigma=f_c'$	1	36.222	38	952	2.243
	2	37.843	41	932	2.098
	3	36.501	40	900	1.899
	4	36.398	39	963	2.255
Vertex at $\epsilon=0.45\%$	1	36.980	41	327	1.075
	2	36.291	40	307	0.991
	3	37.482	42	333	1.181
	4	37.092	41	319	1.066

The tests are performed in an MTS 220 kip=976.8 kN axial-torsional testing machine operated by digital closed-loop control. The stiffness of the machine suffices to keep the present test stable. The precise value of the stiffness of the machine with the platens and the glue is irrelevant because the displacements are measured directly on the specimen.

The experimental results are tabulated in Table 1 and plotted in Figs. 5–11. The vertical error bars indicate the spread of the individual results and the data points are the averages. The mean compressive strength and Young's modulus of the specimens are found to be $f_c'=40$ MPa and $E=36{,}900$ MPa, respectively. The average initial rotational stiffnesses starting at the compression peak and in the postpeak are found to be 936.8 kN m/rad and 322.8 kN m/rad, respectively. In the initial stages of proportional loading, the response of concrete is linearly elastic and the average initial rotational stiffness for this type of loading is found to be 1431 kN m/rad. This means that, when the switch to torsion occurs at the peak, the initial rotational stiffness is approximately 65% of the elastic stiffness, and when in the postpeak, approximately 23% of the elastic stiffness. Obviously, the observed vertex effect is enormous.

Review of Microplane Model M4 for Concrete

The basic idea of the microplane model is to characterize the material behavior not in terms of tensors but in terms of vectors of the stresses and strains acting on a plane of various orientation in the material, since 1984 called the ''microplanes.'' The contri-

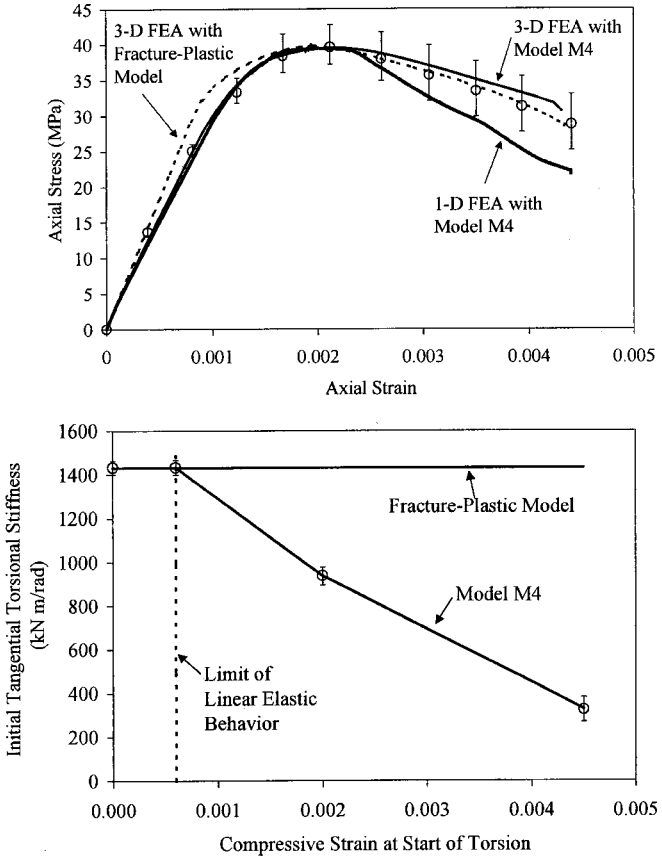

Fig. 5. Bottom: Vertex effect as revealed by initial tangential torsional stiffness at various axial compressive strains. Top: Corresponding axial compressive stress-strain curve [the data points, representing the average test results, and the error bars, representing the spread of test results, are compared to one- and three-dimensional finite element simulations with the original (unadjusted) microplane model M4 and the plastic-fracture model (with one adjusted parameter)]

butions from the microplanes of all possible orientations at a given point of the material are then suitably combined to obtain the continuum response at that point. This idea can be traced back to Taylor (1938) who proposed it for the plasticity of polycrystalline metals where this type of model was known for a long time as the slip theory of plasticity (Batdort and Budianski 1949; see the reviews in Bažant et al. 2000 and in Brocca and Bažant 2000a,b). This name became unsuitable when the model was extended at Northwestern University to damage and cracking, and the term "microplane model" was coined in 1984. Microplane model M4 is the latest in a long sequence of microplane models for concrete developed at Northwestern Univ. since 1983 (Bažant et al. 2000).

The strain vector on a microplane whose unit normal is given by **n** with components n_i at a point in the material is the projection of the strain tensor ϵ_{ij}, which represents a kinematic constraint of the microplane

$$\epsilon_N=\epsilon_{ij}n_in_j, \quad \epsilon_L=\epsilon_{ij}(l_in_j+n_il_j)/2, \quad \epsilon_M=\epsilon_{ij}(m_in_j+n_im_j)/2 \tag{1}$$

The Latin lowercase subscripts refer to Cartesian coordinates x_i ($i=1,2,3$); repeated indices imply summation; ϵ_N=normal strain on the microplane; ϵ_L, ϵ_M=shear strains on the microplane in the directions of two mutually orthogonal unit vectors **l** and **m** both normal to $\vec{n}$ which are generated in advance randomly so as to

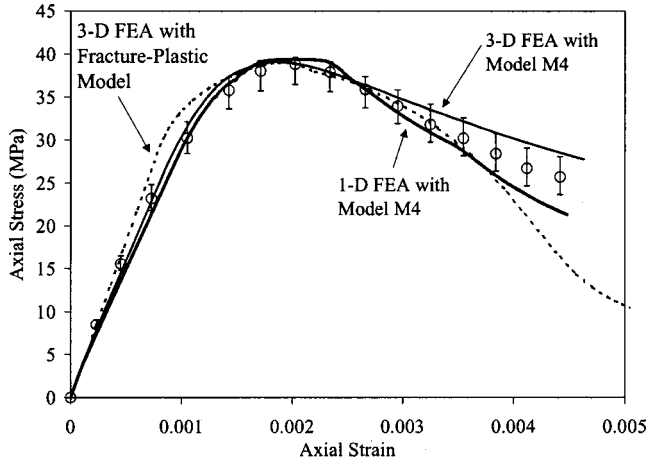

Fig. 6. Axial compressive response to proportional loading as obtained from the tests, and comparisons to one- and three-dimensional finite element simulations

minimize the directional bias. It is useful to also introduce $\epsilon_V=\epsilon_{kk}/3$=volumetric strain for small strains, which is the same for all microplanes.

The kinematic constraint is required due to the occurrence of strain softening of concrete, while a static constraint can be used in Taylor-type models for hardening plasticity of metals [reviewed in Brocca and Bažant (2000a,b) and Jirásek and Bažant (2002)]. A volumetric-deviatoric split of the microplane constitutive relation is introduced,

$$\epsilon_N=\epsilon_D+\epsilon_V. \tag{2}$$

The purpose of this split is to achieve the full thermodynamically admissible range (−1, 0.5) of Poisson's ratio of isotropic materials. Another purpose of this split is to allow simulating both the uniaxial compression tests, in which there is a peak followed by softening, and the tests of hydrostatic pressure (or uniaxial compression strain), in which no peak is ever reached. The difference between these two types of tests is characterized by the spreading strain ϵ_S of the microplane (the mean normal strain among all the

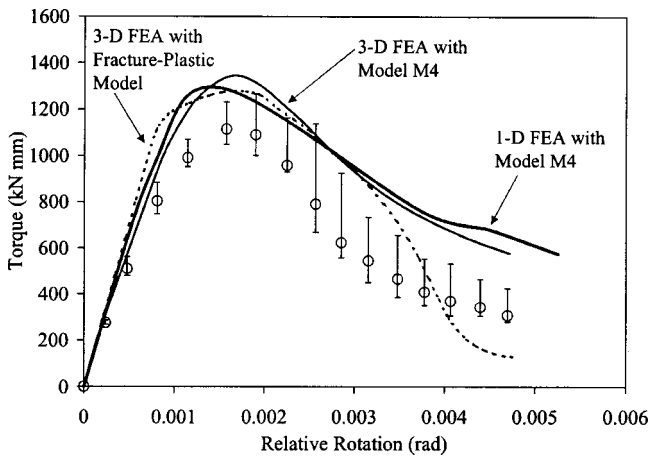

Fig. 7. Rotational response to proportional loading as obtained from the tests, and comparisons to one- and three-dimensional finite element simulations

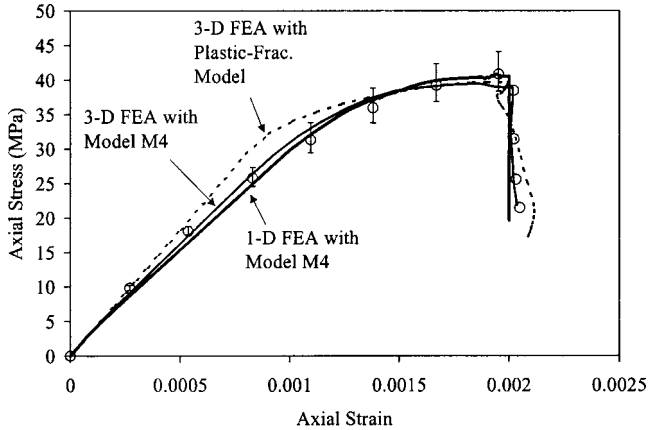

Fig. 8. Axial compressive response to a loading path with a vertex at peak (at $\sigma = f_c'$) as obtained from the tests, and comparisons to one- and three-dimensional finite element simulations

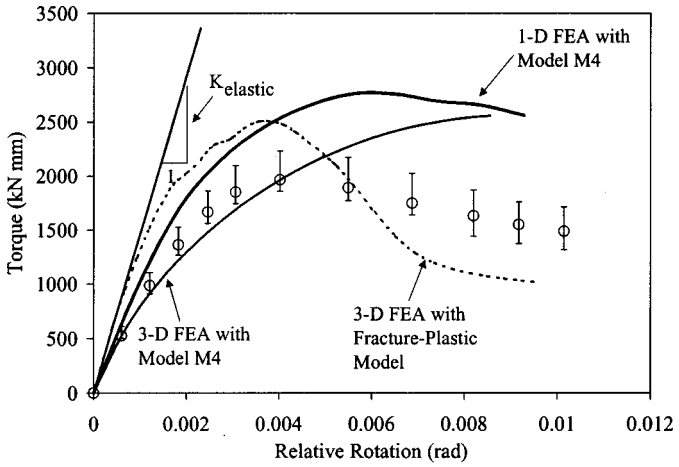

Fig. 9. Rotational response to a loading path with a vertex at peak (at $\sigma = f_c'$) as obtained from the tests, and comparisons to one- and three-dimensional finite element simulations

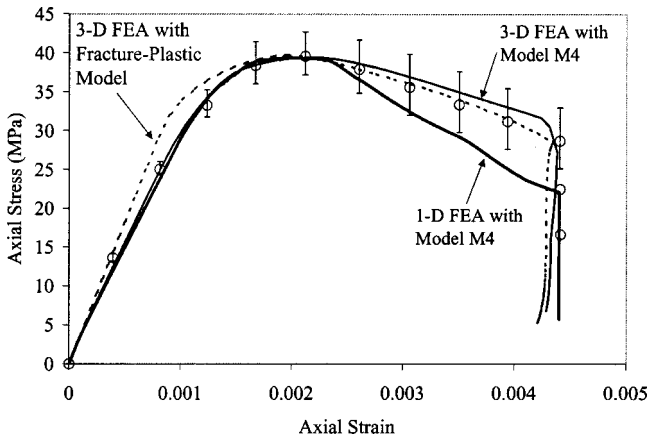

Fig. 10. Axial compressive response to a loading path with a vertex at postpeak (at $\epsilon = 0.45\%$) as obtained from the tests, and comparisons to one- and three-dimensional finite element simulations

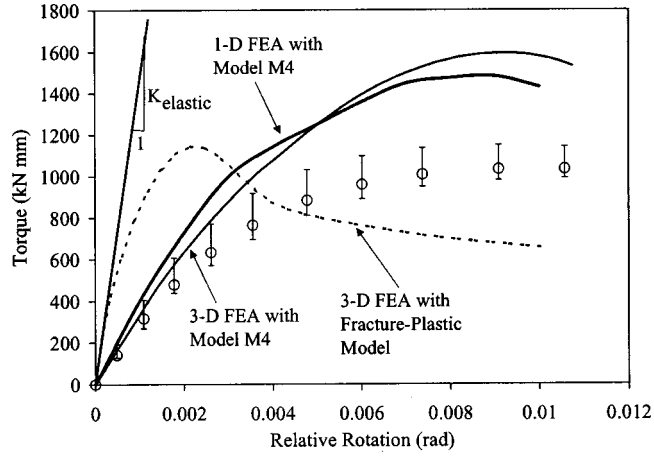

Fig. 11. Rotational response to a loading path with a vertex at postpeak (at $\epsilon = 0.45\%$) as obtained from the tests, and comparisons to one- and three-dimensional finite element simulations

directions within the microplane) which depends on this split because $\epsilon_V = \frac{2}{3}(\epsilon_N - \epsilon_S)$. The elastic response is defined on the microplane level as

$$\sigma_D = E_D \epsilon_D, \quad \sigma_V = E_V \epsilon_V, \quad \sigma_L = E_T \epsilon_L, \quad \sigma_M = E_T \epsilon_M \tag{3}$$

where ϵ_N, ϵ_V, ϵ_L, and ϵ_M are obtained using the kinematic constraint given by Eq. (1) and ϵ_D by Eq. (2). The elastic moduli on the microplane are given by $E_D = E_T = E/(1+\nu)$ and $E_V = E/[3(1-2\nu)]$, where E = Young's modulus and ν = Poisson's ratio (see Bažant et al. 1996a). In the inelastic range, the constitutive laws on the microplane are defined using strain-dependent yield limits, called the stress-strain boundaries, which are given by

$$\begin{gathered} \sigma_N = \mathcal{F}_N(\epsilon_N), \quad \sigma_D = \mathcal{F}_D(\epsilon_D), \quad \sigma_V = \mathcal{F}_V(\epsilon_V) \\ \sigma_L = \mathcal{F}_T(\epsilon_L), \quad \sigma_M = \mathcal{F}_T(\epsilon_M) \end{gathered} \tag{4}$$

and impose bounds that can never be exceeded by the stress. The elastic stress increments on the microplane, as calculated from Eq. (3), are not allowed to reach beyond the corresponding stress-strain boundary given in Eq. (4). If, in a loading step, the stress would exceed the boundary, a stress drop to the boundary is carried out at constant strain.

Finally, equilibrium between the stress tensor σ_{ij} and the stresses on the microplanes is enforced in a weak sense, by using the principle of virtual work over a unit hemisphere. This yields

$$\sigma_{ij} = \frac{3}{2\pi} \int_\Omega \left[\sigma_D \left(n_i n_j - \frac{\delta_{ij}}{3} \right) + \frac{\sigma_L}{2} (n_i l_j + n_j l_i) + \frac{\sigma_M}{2} (n_i m_j + n_j m_i) \right] d\Omega + \sigma_V \delta_{ij} \tag{5}$$

where δ_{ij} is Kronecker's delta. The integration in Eq. (5) must be performed numerically, which is done by Gaussian quadrature over a finite number of integration points over a unit sphere, corresponding to the microplane normals. The most efficient Gaussian quadrature formula is Bažant and Oh's 21-point formula whose errors in the hardening range are not graphically discernible and in the strain softening range lead to a scatter band of a maximum width of about 5% (Bažant and Oh 1986). The present simulations utilized a 28-point formula of Stroud (1971) which is slightly less efficient but slightly more accurate. The numerical

algorithms for this model in the small strain range using explicit dynamic or implicit finite element drivers are presented in Caner and Bažant (2000).

Model M4 was calibrated with a wide range of uni-, bi-, and triaxial test data (Caner and Bažant 2000). It has only two pairs of free parameters which can be easily adjusted to match the given basic properties of concrete. A simple calibration procedure is given in that paper. For the concrete used in the tests, the values of these free parameters, which characterize the boundaries in Eq. (4) and are defined in Bažant et al. (2000), are identified as $k_1 = 0.00013$, $k_2 = 500$, $k_3 = 15$, $k_4 = 150$; and the Young's modulus is $E = 36{,}900$ MPa.

One-Dimensional Analysis Using Model M4

The axial displacement, u, at the top of the specimen is prescribed and incremented in small steps. In a simplified one-dimensional analysis, the end effects and possible damage localizations are neglected, which means that the specimen is assumed to behave approximately in the same manner as an infinitely long cylinder in which each cross section is in the same stress and strain state. Thus the axial normal strain is assumed to be uniform and has the value $\epsilon = u/L$. When the relative rotation over the gauge length is ϕ, the shear strains γ vary linearly with the radial coordinate r; $\gamma = \phi r/L$. The distribution of the axial normal stresses along the radius is uniform only during the uniaxial compression. As a result of the shear-volume coupling of the inelastic behavior of concrete (particularly the volume dilatancy due to shear), which is well captured by the microplane model, the axial stress distribution becomes nonuniform during torsion. The mesh is one-dimensional along the radius and consists of a row of N axisymmetric finite elements of radial dimension $\Delta r = R/N$, where R is the radius of cylinder. The expression for the torque T and its discrete approximation is

$$T(\phi) = \int_0^R \tau\left(\frac{\phi r}{L}\right) r 2\pi r \, dr \approx 2\pi(\Delta r)^3 \sum_{n=1}^{N} \tau\left(\frac{\phi n \Delta r}{L}\right) n^2 \quad (6)$$

For proportional loading, $u/\phi = \text{const}$, but the ratio of axial to shear strains is not constant because the shear strains vary along the radial coordinate.

Three-Dimensional Finite Element Simulations

To get a more realistic picture, three-dimensional finite element analysis of the test cylinder is carried out using microplane model M4 (Bažant et al. 2000). The parameters used for model M4 (with a meaning defined in Bažant et al. 2000) are $E = 36.9$ GPa, $\nu = 0.18$ (Poisson ratio), $k_1 = 130 \times 10^{-6}$, $k_2 = 500$, $k_3 = 15$, and $k_4 = 150$. Parameters $k_1, \ldots, k_4$ are the free parameters of model M4 calibrated for the given concrete as described in Caner and Bažant (2000). The number of discrete microplanes is $n_{\text{mp}} = 28$, which corresponds to Stroud's (1971) optimal Gaussian integration formula for a hemisphere. Note that the fracture energy and the effective fracture process zone length corresponding to model M4 could be obtained by the size effect method (e.g., Bažant and Planas 1998), after simulating similar fracture tests of three different sizes.

For the sake of comparison, it was decided to also conduct the finite element analysis with one of the sophisticated damage-plasticity models for concrete formulated in the classical way, that is, in terms of the stress and strain tensors and their invariants (Bažant and Kim 1979; Lin et al. 1987; Červenka et al. 1998). The recent model of Červenka et al. (1998), an advanced model that has been successfully used in many practical problems, has been selected.

This model is based on the classical orthotropic smeared crack model for tension and a plasticity model for compression. The plasticity model uses a nonassociated plastic flow rule and the three-parameter yield surface of Menetrey and Willam (1995). The smeared crack model employs the rotating crack approach, i.e., the distributed cracks are imagined to rotate so as to remain aligned with the principal strain directions. This hypothesis was much discussed in the early 1980s (Jirásek and Bažant 2002), with the conclusion that it is better than assuming the crack direction to be fixed at the beginning of strain softening. The crack rotation concept is necessary because simultaneous cracks of at most three different orientations are allowed. This simplifying concept substitutes for the fact that cracks of one orientation are closing while those of another orientation are opening. By contrast, the simplifying hypothesis of crack rotation is unnecessary in the microplane model because there can be as many crack orientations as there are discrete microplanes.

The parameters used for the model of Červenka et al. (1998) are $\beta = 0$, $f_c' = -40$ MPa, $f_t' = 3.13$ MPa, $\nu = 0.18$, $E = 36.9$ GPa, $G_f = 0.1506$ MPa mm, $\epsilon_c^p = -0.001075$, $w_d = -0.2$ mm, $f_c^0 = -30$ MPa, and $e = 0.52$ where β defines the return direction of the plasticity model with respect to the direction perpendicular to the hydrostatic axis in Haigh–Westergaard coordinates, f_c' is the unconfined compressive strength, f_t' is the tensile strength, G_f is Mode I fracture energy, ϵ_c^p is the plastic strain at $\sigma = f_c'$ in an unconfined compression test, w_d is the displacement beyond which $\sigma \approx 0$ in an unconfined compression test, f_c^0 defines the onset of nonlinear behavior in compression, and e defines the shape of the failure surface in the deviatoric plane.

A three-dimensional mesh of 2,484 elements and 3,000 nodes is used. It covers the entire specimen since a nonsymmetric localization of softening damage must be expected. The boundary conditions at the top of the cylinder are prescribed as the axial displacements and horizontal displacements due to rotation of the platens considered as a rigid body. In each loading step, the boundary displacement and rotation are adjusted so as to match the relative displacements and rotations recorded during the tests at the attached steel rings carrying the LVDTs. The bottom boundary of the cylinder is kept fixed.

The load path with a sudden switch from compression to torsion is simulated by applying first uniform vertical displacement increments at the top face nodes while these nodes are fixed in horizontal radial and angular directions. After a specified axial displacement between the rings with LVDTs is reached, horizontal angular displacements corresponding to rigid-body rotation increments of the platens are prescribed at the top boundary nodes while keeping the axial relative displacement of the attached rings with LVDTs constant. These displacements were specified as 0.23 and 0.51 mm for the load paths with a switch at peak and at postpeak, respectively. During the rotational loading, the top boundary nodes are assigned also appropriate vertical displacement increments such that the vertical relative displacement of the rings would remain approximately constant.

The load path with proportional loading is prescribed at the top boundary nodes of the cylinder in the form of axial and rotational displacements corresponding to the axial and rotational rigid-body displacements of the platen which are in each step adjusted such that the ratio of the relative axial displacement of

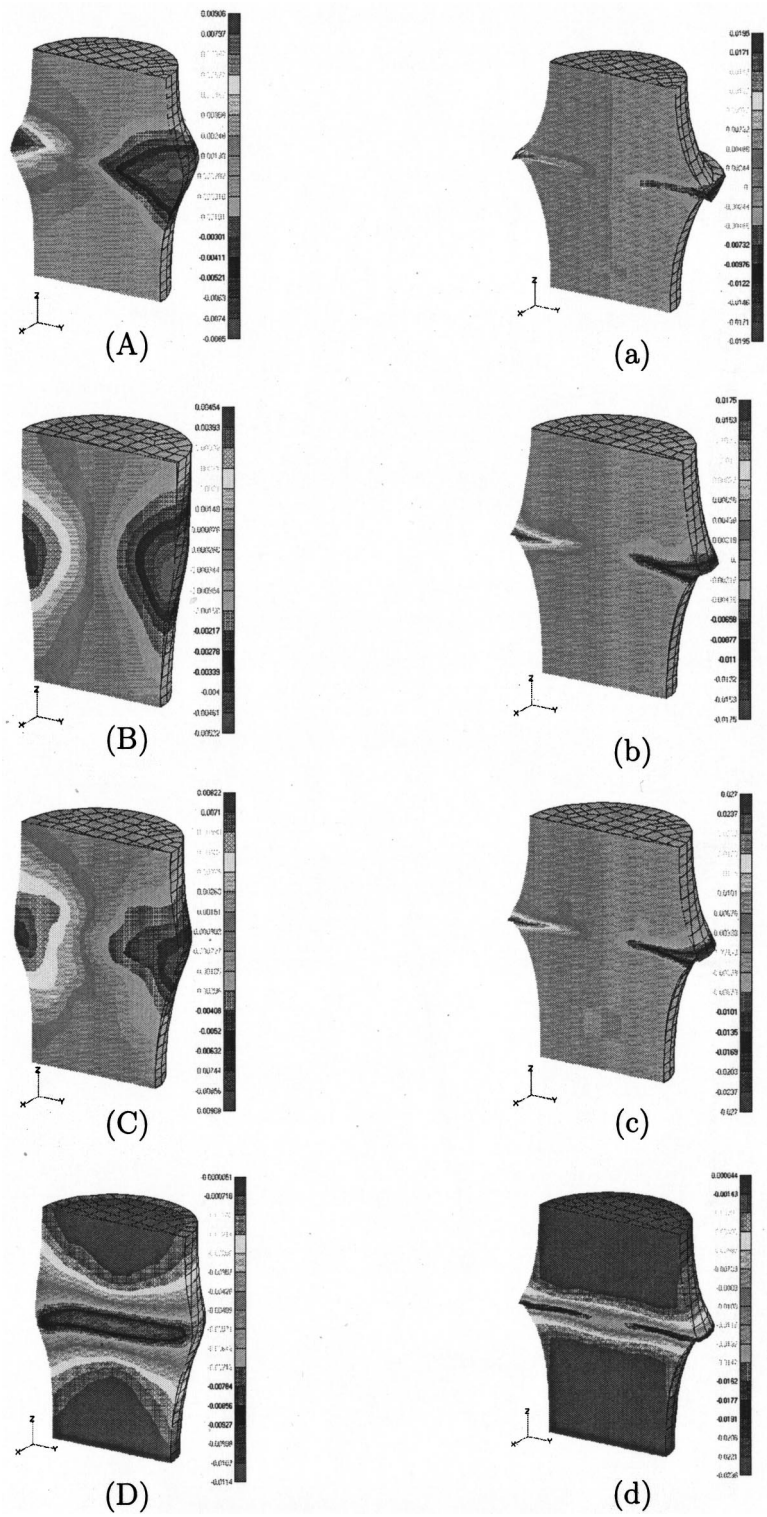

Fig. 12. Deformed shapes obtained using model M4 (on the left) and the fracture-plastic model (on the right) for three loading paths: (A, a) proportional loading; (B,b) vertex at peak; (C,c,D,d) vertex in postpeak (at $\epsilon_{zz}=0.45\%$), showing strain contours for γ_{xz} (A,B,C,a,b,c), and for maximum principal strain ϵ_I (D, d)

rings to their relative rotation be kept fixed at approximately 100 mm/rad in each loading step.

Results of Finite Element Simulations and Comparisons with Data

The results of the finite element analyses and their comparisons with tests are shown in Figs. 5–12. Fig. 5 presents the main result of this study—the reduction of the initial torsional stiffness caused by increasing compressive strain, which represents the essence of the vertex effect. Obviously, the vertex effect in concrete is very strong. The curves calculated with microplane model M4 are seen to provide excellent predictions of the vertex effect. On the other hand, the plastic-fracture model gives no vertex effect (i.e., no stiffness reduction), which is an inherent property of all

the classical formulations of constitutive models in terms of tensors and their invariants.

Figs. 6 and 7 show the axial stress-strain and torque-rotation responses for proportional loading. The averages of all the measurements for identical tests are shown as the solid lines and the statistical scatter is marked by the vertical error bars indicating the spread of the results. This spread should be taken into account in judging the quality of the model predictions or fits.

The test data and the numerical simulations of the axial stress-strain and torque-rotation responses to the loading path with a compression torsion switch at peak ($\sigma = f_c'$) are compared in Figs. 8 and 9, respectively. The responses calculated from both models for large rotations do not match the test data accurately. But it must be kept in mind that the curves for model M4 represent a complete prediction (except for the setting of the correct strength value by means of parameter k_1, the M4 parameters were taken the same as obtained by Caner et al. 2000). On the other hand, the plastic-fracture model represents only a partial prediction because, in addition to setting the strength value, one model parameter was adjusted to optimize the postpeak slope.

Either model could doubtless be made to fit the large-rotation response closely if many model parameters were adjusted, but then the match of other types of test data (as described in Caner et al. 2000) would be jeopardized. The main point of this paper, however, is that the initial torsional stiffness cannot be controlled by adjusting model parameters.

For proportional loading paths, the fracture-plastic model and the microplane model should, in theory, be able to perform equally well. Model M4 nevertheless performs slightly better.

The distributions of the shear strains γ_{xz} in the specimens loaded proportionally are shown in Figs. 12(A and a) obtained with model M4 and the fracture-plastic model, respectively. Clearly, the model M4 predicts a more uniform damage than the fracture-plastic model does. With the fracture-plastic model, damage tends to localize to a relatively small volume within the specimen. This contrast between the two models prevails for loading with a sudden switch from compression to torsion at the peak, as seen in Figs. 12(B and b) obtained with model M4 and the fracture-plastic model, respectively, and also for loading with a sudden switch in the postpeak [Figs. 12(C and c) obtained with the model M4 and the fracture-plastic model, respectively].

The distributions of the maximum principal strains ϵ_I are shown in Figs. 12(D and d), as obtained with model M4 and the fracture-plastic model, for the loading path with a switch in the postpeak. Once again, the distribution of damage as predicted by the model M4 is more uniform compared to that predicted by the fracture-plastic model.

The way the microplane model captures the vertex effect is that it involves very many simultaneous yield surfaces (called boundaries), in effect creating the situation depicted in Fig. 1(d). In model M4, there are 3 independent boundaries on each microplane—deviatoric, volumetric, and shear frictional. At least 21 microplanes must be used, which provides at least 63 simultaneous (strain-dependent) yield surfaces. Each of them can independently load or unload, which gives in theory 2^{63} (or 10^{19}) possible combinations of loading and unloading. In a kinematically constrained microplane model such as M4, the main contribution to the vertex effect at a sudden change in loading path direction arises from a change in the loading-unloading combination among the deviatoric, volumetric, and shear-frictional boundaries on each microplane. On the other hand, in a statically constrained microplane model (which is effective for metals but cannot handle softening damage), a large contribution comes also from a change in the loading-unloading combination among all the microplanes (Brocca and Bažant 2000a) (this becomes the only source of vertex effect in the case of a statically constrained microplane model for metal plasticity in which there is only one yield surface on each microplane).

Conclusions

1. By using a state-of-the art testing machine capable of a sudden switch from compression to torsion and on-specimen gauges with a fast feedback, the vertex effect in the response of concrete to nonproportional loading paths in the stress space has been documented experimentally.
2. At peak compressive load, the vertex effect is strong, and in postpeak very strong. Compared to the elastic torsional stiffness, the initial torsional stiffness after a sudden switch from compression to torsion is reduced to 65% when the torsion begins at compression load peak, and to 23% when the torsion begins at a postpeak state at which the axial load has decreased to 70% of the peak load.
3. The experimental data obtained are modeled using two state-of-the-art but conceptually completely different models. One is microplane model M4, and the other is a fracture-plastic model, a state-of-art tensorial model based on invariants.
4. The initial torsional stiffness after a sudden switch from compression to torsion is predicted by microplane model M4 quite accurately, and without any adjustment of the material parameters previously calibrated by other tests. This demonstrates the microplane model M4 can predict the vertex effect, and does so correctly.
5. The capability of predicting the vertex effect is due to fact that the model implies many simultaneous, independently activated (strain-dependent) yield surfaces on the microplanes and has also independent yield surfaces for volumetric, deviatoric, and shear response on each microplane. It is the interaction of these surfaces that produces the vertex effect.
6. The classical invariant-based tensorial models employing only a few yield (or loading potential) surfaces, represented in the present simulation by an advanced model, the fracture-plastic model, are inherently incapable of simulating the vertex effect, and more generally the response to highly nonproportional loading paths. This is documented by the fact that they incorrectly predict the initial torsional stiffness after the switch to be the elastic torsional stiffness.
7. The microplane model prediction of overall response to torsional loading after a switch from compression to torsion is less accurate. This overall response is hardly better than that of the plastic-fracture model. Note, however, that the former is a true prediction, in which no model parameters, except the setting of compression strength, have been adjusted, while the latter is a partial prediction since one parameter had to be adjusted to obtain a reasonable postpeak softening slope in uniaxial compression.

Acknowledgments

Grateful appreciation is due to the U.S. Army Engineer Waterways Experiment Station (WES), Vicksburg, Miss., for funding the work of the second writer under Contract Nos. DACA39-94-C-0025 and DACA42-00-C0012 with Northwestern University. F. C. Caner wishes to thank the U.S. National Science Foundation

for funding his doctoral research under Grant No. CMS-9713944 to Northwestern University. The contribution of Jan Červenka was partly supported by the Czech Grant Agency under Contract No. 103/99/0755.

References

Batdorf, S. B., and Budianski, B. (1949). ''A mathematical theory of plasticity based on the concept of slip.'' *Technical Note No. 1871*, National Advisory Committee for Aeronautics, Washington, D.C.

Bažant, Z. P. (1978). ''Endochronic inelasticity and incremental plasticity.'' *Int. J. Solids Struct.*, 14, 691–714.

Bažant, Z. P. (1980). ''Work inequalities for plastic-fracturing materials.'' *Int. J. Solids Struct.*, 16, 870–901.

Bažant, Z. P. (1983). ''Comment on orthotropic models for concrete and geomaterials.'' *J. Eng. Mech.*, 109(3), 849–865.

Bažant, Z. P., and Baweja, S. (2000). ''Creep and shrinkage prediction model for analysis and design of concrete structures: Model B3.'' *Adam Neville Symposium: Creep and Shrinkage—Structural Design Effects*, ACI SP-194, A. Al-Manaseer, ed., Am. Concrete Institute, Farmington Hills, Mich., 1–83.

Bažant, Z. P., Caner, F. C., Carol, I., Adley, M. D., and Akers, S. A. (2000). ''Microplane model M4 for concrete: I. Formulation with work-conjugate deviatoric stress.'' *J. Eng. Mech.*, 126(9), 944–953.

Bažant, Z. P., and Cedolin, L. (1991). *Stability of structures: Elastic, inelastic, fracture and damage theories*, Oxford University Press, New York.

Bažant, Z. P., and Kim, S. S. (1979). ''Plastic-fracturing theory for concrete.'' *J. Eng. Mech. Div.*, 105(EM-3), 407–428.

Bažant, Z. P., and Oh, B.-H. (1986). ''Efficient numerical integration on the surface of a sphere.'' *Z. Angew. Math. Mech.*, 66(1), 37–49.

Bažant, Z. P., and Planas, J. (1998). *Fracture and size effect in concrete and other quasibrittle materials*, CRC Press, Boca Raton, Fla.

Bertsch, P. K., and Findley, W. N. (1962). ''An experimental study of yield surfaces-corners, normality, Bauschinger and allied effects.'' *Proc. 4th U.S. National Congr. of Applied Mechanics*, ASME, New York, 893–907.

Bleich, F. (1952). *Buckling strength of metal structures*, McGraw-Hill, New York.

Budianski, B. (1959). ''A reassessment of deformation theories of plasticity.'' *Trans. ASME, J. Appl. Mech.*, 26, 259–264.

Budianski, B., Dow, N. F., Peters, R. W., and Ghephard, R. P. (1951). ''Experimental studies of polyaxial stress-strain laws of plasticity.'' *Proc., 1st U.S. National Congr. of Applied Mechanics*, ASME, New York, 503–512.

Brocca, M., and Bažant, Z. P. (2000a). ''Microplane constitutive model and metal plasticity.'' *Appl. Mech. Rev.*, 53(10), 265–281.

Brocca, M., and Bažant, Z. P. (2000b). ''Microplane finite element analysis of tube-squash test of concrete with shear angles up to 70°.'' *Int. J. Numer. Methods Eng.*, in press.

Caner, F. C., and Bažant, Z. P. (2000). ''Microplane model M4 for concrete: II. Algorithm and Calibration.'' *J. Eng. Mech.*, 126(9), 954–961.

Červenka, J., Červenka, V., and Eligehausen, R. (1998). ''Fracture-plastic material model for concrete, Application to analysis of powder actuated anchors,'' *Proc., 3rd Int. Conf. on Fracture Mechanics of Concrete Structures* (FraMCoS-3, held in Gifu), H. Mihashi and K. Rokugo, eds., Vol. 2, Aedificatio Publishers, Freiburg, Germany, 1107–1117.

Christoffersen, J., and Hutchinson, J. W. (1979). ''A class of phenomenological corner theories in plasticity.'' *J. Mech. Phys. Solids*, 27, 465–487.

Dougill, J. W. (1976). ''On stable progressively fracturing solids.'' *Z. Angew. Math. Phys.*, 27, 423–437.

Drucker, D. C. (1950). ''Some implications of work hardening and ideal plasticity.'' *Q. Appl. Math.*, 7, 411–418.

Gerard, G., and Becker, H. (1951). ''Column behavior under conditions of impact.'' *J. Aerosp. Sci.*, 19, 58–65.

Gerard, G., and Becker, H. (1957). ''Handbook of structural stability: Part I, Buckling of flat plates.'' *NACA Technical Note* No. 3781.

Hughes, T. J. R., and Shakib, F. (1986). ''Pseudo-corner theory: A simple enhancement of J_2-flow theory for applications involving nonproportional loading.'' *Eng. Comput.*, 3, 116–20.

Ivey, H. J. (1961). ''Plastic stress-strain relations and yield surfaces for aluminum alloys.'' *J. Mech. Eng. Sci.*, 3, 15–31.

Jirásek, M., and Bažant, Z. P. (2002). *Inelastic analysis of structures*. Wiley, London.

Koiter, W. T. (1953). ''Stress-strain relations, uniqueness and variational theorems for elastic-plastic material with a singular loading surface.'' *Q. Appl. Math.*, 11(3), 29–53.

Lin, F.-B., Bažant, Z. P., Chern, J.-C., and Marchertas, A. H. (1987). ''Concrete model with normality and sequential identification.'' *Comput. Struct.*, 26(6), 1011–1025.

Menetrey, P., and Willam, K. J. (1995). ''Triaxial failure criterion for concrete and its generalization.'' *ACI Struct. J.*, 92(3), 311–318.

Naghdi, P. M., Essenburg, F., and Koff, W. (1958). ''An experimental study of initial and subsequent yield surfaces in plasticity.'' *J. Appl. Mech.*, 25, 201–209.

Phillips, A. (1972). ''Solution of plastic buckling paradox.'' *AIAA J.*, 10, 951–953.

Phillips, A. (1986). ''A review of quasi-static experimental plasticity and viscoplasticity.'' *Int. J. Plast.*, 2, 315–328.

Phillips, A., and Gray, G. A. (1961). ''Experimental investigation of corners in the yield surface.'' *J. Basic Eng.*, 83, 275–289.

Rice, J. R. (1975). ''On the stability of dilatant hardening of saturated rock masses.'' *J. Geophys. Res.*, 80(11), 1531–1536.

Rice, J. R. (1976). ''The localization of plastic deformation.'' *Preprints, 14th Congr. of Int. Union of Theoretical and Applied Mechanics* (held in Delft), W. Koiter, ed., North-Holland, Amsterdam, 207–220.

Rudnicki, J. W., and Rice, J. R. (1975). ''Conditions for the localization of deformation in pressure sensitive dilatant materials.'' *J. Mech. Phys. Solids*, 23, 371–394.

Sanders, J. L. (1954). ''Plastic stress-strain relations based on linear loading functions.'' *Proc., 2nd U.S. National Congr. of Applied Mechanics*, Univ. of Michigan, Ann Arbor, 455–466.

Stroud, A. H. (1971). ''Approximate Calculation of Multiple Integrals,'' Prentice-Hall, Englewood Cliffs, N.J.

Taylor, G. I. (1938). ''Plastic strain in metals.'' *J. Inst. Met.*, 62, 307–324.